

Research Article

## Corrosion Mechanisms Caused on a Submerged Nozzle Applied in Steel Billet Production by Mold Fluxes with and without Fluorine

M.V. Peirani, E. Brandaleze

High Temperature Physicochemistry, Metallurgy Department-DEYTEMA Centre, Facultad Regional San Nicolás, Universidad Tecnológica Nacional, Colón 332 (2900), San Nicolás, Argentina

### \*Corresponding author

M.V. Peirani

Email: [vpeirani@frsn.utn.edu.ar](mailto:vpeirani@frsn.utn.edu.ar)

**Abstract:** Alumina-graphite ( $\text{Al}_2\text{O}_3\text{-C}$ ) refractories are used as immersion nozzles for the continuous casting of steel. Carbon containing refractory materials have been widely used due to their excellent mechanical properties, thermal shock resistance and corrosion resistance. The life of these nozzles are limited by the localized corrosion, which occurs at the melt mold flux-metal interface. These refractory pieces are constituted by a body of alumina-graphite ( $\text{Al}_2\text{O}_3\text{-C}$ ) with an insert of zirconia-graphite ( $\text{ZrO}_2\text{-C}$ ). The insert is placed in the bottom of the nozzle to protect the vulnerable zone from chemical attack. For this reason, the deep understanding of the mold fluxes effect on the wear mechanisms of the nozzles is relevant in order to avoid premature damage and contribute to decrease the cost of black refractories in the industry. In this paper, the nozzle selected for the study was characterized considering the chemical composition determination (integrating different instrumental techniques), the thermal behaviour (obtained by thermal analysis DTA/TGA), physical properties (such as density and apparent porosity) and microstructural characteristics (carried out by optical microscopy). The corrosion mechanisms produced by a mold flux with 2.6% of fluorine content on one ( $\text{Al}_2\text{O}_3\text{-C}$ ) nozzle is studied by a post mortem study and it is compared with a static corrosion test carried out with the same fluorine flux and besides with another free fluorine mold flux. The microstructural study was performed by light (OM) and scanning electron microscopy (SEM). The information was correlated with results of the thermodynamic corrosion simulation applying the software Fact Sage 7.1. Mould fluxes structural characteristics and physical properties such as surface tension, viscosity, fluidity and the melting behaviour allows to justify the corrosion effects obtained.

**Keywords:** submerged nozzles, alumina-graphite, mold powders, corrosion, continuous casting.

### INTRODUCTION

In the steel continuous casting process, conventional commercial mold fluxes with fluorine are used. Fluorine has significant influence on the physical properties and performance of the process. However, the gases emissions produced affect the environment. For this reason, new mold fluxes with low fluorine content or free fluorine are designed in order to improve casting conditions and to protect the human health as well as the environmental. In consequence, it is relevant to study the effects of the new mold fluxes on nozzle life in service in order to prevent premature damage and decrease the costs of the refractories used [1].

The corrosion behavior of refractories is important for the performance in any application area. Corrosion is the chemical property of refractories dependent on the chemical affinity, densification

behaviour, pore character (amount, size, and distribution), impurities amount and types, strength behaviour, among others factors [2]. Lee and Zhang in [3], describe the attack of the refractories as a complex phenomenon involving not only chemical wear (corrosion), they consider the combination of physical and mechanical wear. The corrosion affects the internal structure of the nozzles and all the properties. For these reason, it is important a deep understanding and evaluation of the problem in order to prolong the nozzle life in service avoiding the interruption in the continuous casting production and promoting a decrease the costs on refractories.

One of the nozzle refractory materials with optimum performance is the alumina-graphite ( $\text{Al}_2\text{O}_3\text{-C}$ ) with phenolic resin as binder. These refractory pieces are constituted by a body of alumina-graphite

(Al<sub>2</sub>O<sub>3</sub>-C), with an insert of zirconia-graphite (ZrO<sub>2</sub>-C). The insert is placed in the bottom of the nozzle to protect the vulnerable zone from chemical attack. The use of ZrO<sub>2</sub> is justified due to the oxide high melting point, the chemically inert and special mechanical properties of the material.

Research on mold flux attack of the oxide-graphite submerged entry nozzle refractories was reviewed along years by different authors. There is general agreement that the mechanism involve attack of both the oxide and the carbonaceous binder, but there is some uncertainty about the process of attack of the carbon. There is some debate over the importance of surface tension driven stirring in a system where forced convection rates are high. Mukai in [4] and Hauck and Potschke in [5] have proposed a mechanism for the localized corrosion that occur in the nozzles based on the intense fluid convection at the interface caused by interfacial tension gradients. Qian in [6] report information on the effect of graphite content on decarburization and on the corrosion resistance of zirconia-graphite materials. Brandaleze *et al.* in [7, 8], discuss the impact of the physical properties of mold fluxes on the nozzle wear mechanisms, principally considering the ZrO<sub>2</sub> aggregates degradation by chemical attack.

In this paper the main objective is to contribute on the knowledge of the corrosion mechanisms produced on the (ZrO<sub>2</sub>-C) insert of a nozzle applied in steel billet continuous casting. The corrosive agents selected are two mold fluxes: the flux M1 with 2.6% of fluorine and the flux M2 without fluorine content. The static corrosion tests were carried out with these two mold fluxes and then they were compared with a post mortem sample that was in contact with the flux M1 during their service. The static corrosion test is a comparative test and still useful for assessing the corrosion mechanisms, but not simulates the dynamic process conditions [3]. The post mortem study allows to establish the corrosion mechanisms suffered in the nozzle at process conditions and also to obtain information of the final wear stage. However, in the interpretation of the results is necessary to take into account the importance of dynamics and complexity of the mold flux-nozzle interface evolution along the service.

The characterization of the nozzle material, including chemical and mineralogical composition, structural aspects and physical properties such as apparent density and porosity represent the start point for the corrosion operative mechanisms understanding. In this sense, the evolution of the nozzle materials with temperature also bring useful information. The physical properties behaviour of the mold flux at process conditions such as: viscosity, fluidity and surface

tension need to be correlated. This information is determined by experimental tests and also compared with results obtained by different theoretical models and thermodynamic simulations applying Fact Sage 7.1 [9, 10].

The static corrosion test and post mortem results are analyzed through the information obtained of the structural aspects observed by light and scanning electron microscopy techniques. The chemical composition of the infiltrated phases were determined by SEM with EDS analysis. The evolution of the phases predicted by the thermodynamic simulation is correlated with the structural results. By the thermochemical simulations, the chemical reactions in the system between nozzle and mold flux are justified. All the information is useful to identify the corrosion mechanisms and to predict conditions of the dynamic process that cause the damage in the refractory material.

## MATERIAL AND METHODS

The alumina-graphite nozzle selected for the study is applied in steel billet production. Two specimens are considered: a nozzle (as received) and a post mortem sample used along one campaign in contact with the mold flux M1.

The characterization of the (as received) sample include: the chemical composition determination obtained by X-ray fluorescence spectroscopy and ICP mass spectrometers in combination with X ray diffraction (XRD) and scanning electron microscopy SEM with EDS analysis. The microstructural characteristics were observed by optical microscopy with an OLYMPUS GX 51 microscope and scanning electron microscopy (SEM) FEI QUANTA 200F. Physical properties (such as density and apparent porosity) were determined by Archimedes method. The thermal behaviour was obtained by thermal analysis DTA/TGA using a SHIMADZU DTG-60/60H instrument.

The mold fluxes chemical composition and physical properties were determined by experimental tests in correlation with theoretical models and Fact Sage 7.1 simulation according with the methodology mentioned in [1].

The static corrosion test was performed in an ORL furnace at 1400°C in air atmosphere. The corrosive agent (mold fluxes M1 and M2) were placed into the hole of the crucibles. The microstructural study was carried out on the static corrosion crucibles and the post mortem sample by light microscopy (OM) and scanning electron microscopy (SEM). The information was correlated with results of the thermodynamic corrosion simulation applying the software Fact Sage 7.1.

**RESULTS AND DISCUSSIONS**

**As Received Nozzle Characterization**

The chemical composition results of the alumina-graphite nozzle, involving both parts of the piece (body and insert), was obtained by different instrumental techniques. In Table 1, the main oxides content and carbon content (in % wt.) are detailed. This information is consistent with the crystalline phases identified by X-ray diffraction, see Figures 1 (a) and (b). The body is mainly constituted by alpha Al<sub>2</sub>O<sub>3</sub>

(corundum, A) and graphite (C). A lower content of mullite (3Al<sub>2</sub>O<sub>3</sub>.2SiO<sub>2</sub>, M) and monoclinic zirconia (Z<sub>m</sub>), were also detected. In the insert material, two types of ZrO<sub>2</sub> and the graphite peaks (C) were observed. The cubic zirconia phase (Z<sub>c</sub>) is the principal aggregate component of the insert, whereas a low content of monoclinic zirconia phase (Z<sub>m</sub>) also was detected. In both parts of the nozzle, the graphite peaks detected are consistent with the carbon content (C) informed in the chemical composition.

**Table 1: As received Chemical composition (%wt.), Physical properties and Loss on ignition (LOI) of the nozzle.**

Oxides	SiO <sub>2</sub>	Al <sub>2</sub> O <sub>3</sub>	B <sub>2</sub> O <sub>3</sub>	CaO	ZrO <sub>2</sub>	HfO <sub>2</sub>	MgO	TiO <sub>2</sub>	Fe <sub>2</sub> O <sub>3</sub>	K <sub>2</sub> O	Na <sub>2</sub> O	C
<b>Body</b>	6.77	82.05	2.32	0.12	5.81	0.12	0.22	1.17	0.26	0.06	1.12	23.8
<b>Insert</b>	9.32	0.65	-	3.59	84.41	1.69	0.07	0.17	0.09	-	-	16.0
<b>Physical Properties</b>	<b>Density (g/cm<sup>3</sup>)</b>		≈2.5				<b>LOI<sub>950°C</sub> (%wt.)</b>					
	<b>Apparent Porosity (%)</b>		≈15.8				<b>Body: 24</b>			<b>Insert: 17</b>		

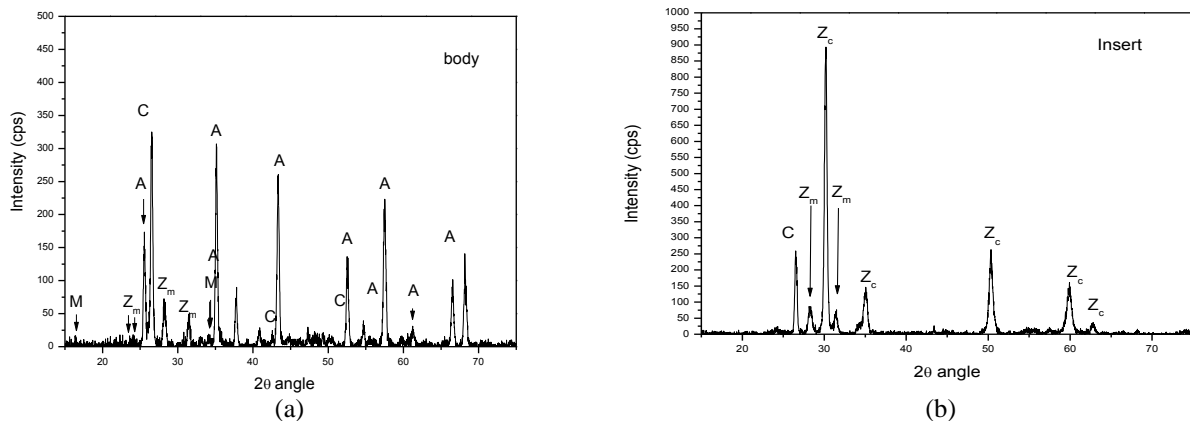


**Fig-1: X-ray diffractograms of the as received nozzle: (a) body material and (b) insert material.**

The structural characterization [11] of the nozzle (as received) was completed with a microstructural study carried out by optical microscopy (OM) and scanning electron microscopy (SEM with EDS). Figure 2 (a) and (b), shows Al<sub>2</sub>O<sub>3</sub> aggregates (A) and flakes of graphite (C) observed by optical

microscopy in the body microstructure in coincidence with the XRD results. Moreover, the presence of AZS (Al<sub>2</sub>O<sub>3</sub>- ZrO<sub>2</sub>- SiO<sub>2</sub>) aggregates is determined. This result corroborate the monoclinic ZrO<sub>2</sub> identified by XRD.

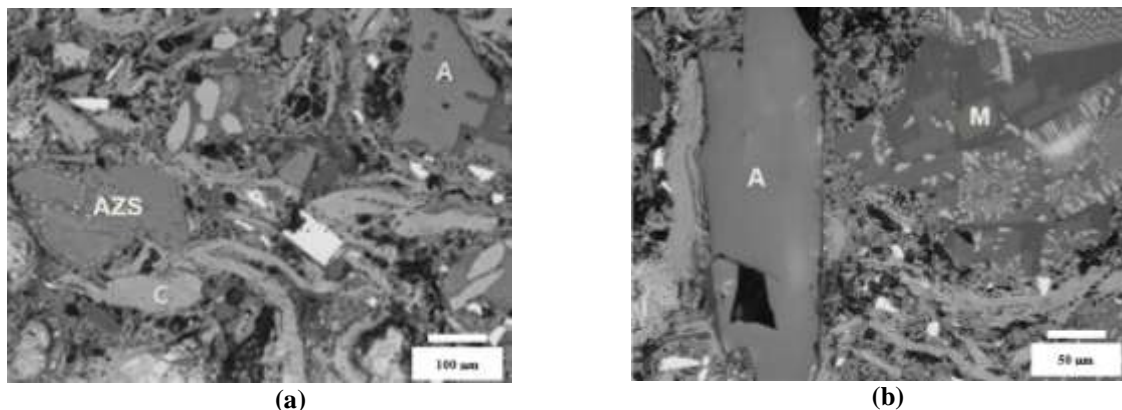


**Fig-2: Body microstructure of the as received nozzle: (a) aggregates of Al<sub>2</sub>O<sub>3</sub> (A), Al<sub>2</sub>O<sub>3</sub>- ZrO<sub>2</sub>- SiO<sub>2</sub> (AZS) and graphite flakes (C), (b) aggregates of Al<sub>2</sub>O<sub>3</sub> (A) and mullite phase (M) identified in the AZS aggregate**

The main reason for the AZS aggregates (containing 67% of  $ZrO_2$  and 33% of  $SiO_2$ ) in the body of the nozzle is to improve the properties because impart special mechanical properties, present low thermal expansion and good thermal stability [2].

In the insert material, graphite flakes (C) and two types of zirconia aggregates were observed: sintered ( $Z_s$ ) and electrofused ( $Z_f$ ) aggregates, see Figure 3(a). These results are consistent with the crystalline phases identified by XRD. However, few aggregates of AZS (not detected by XRD) were also observed by microscopy in the insert microstructure, Figure 3(b).

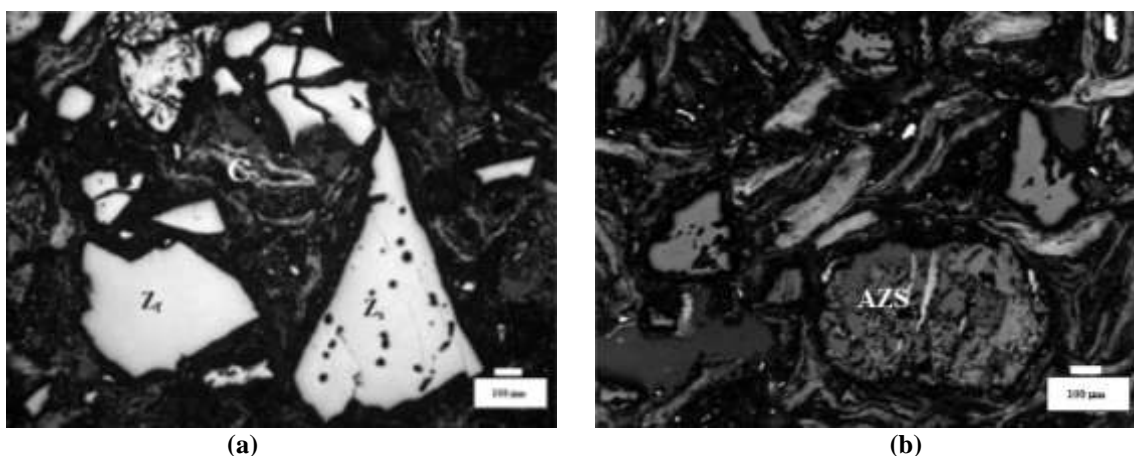


Fig-3: Insert microstructure of the as received nozzle: (a) electrofused zirconia ( $Z_f$ ), sintered zirconia ( $Z_s$ ) aggregates and graphite flakes (C), (b) AZS aggregates identified.

The electrofused zirconia ( $Z_f$ ) with sintered zirconia ( $Z_s$ ) constitute the most chemically stable aggregates with high corrosion resistance against glass melts, slag and liquid metal [2].

The thermal behaviour of the as received nozzle was studied by different experimental techniques. The mass changes associated with temperature increases (up to 1450°C) were determined

by termogravimetry (TGA) on samples of both parts of the nozzle (body and insert). Two step of mass loss were identified in the thermograms carried out in air atmosphere. In the body material, see Figure 4 (a): the step 1 (up to  $\approx 551^\circ C$ ) results in a mass loss of  $\approx 5.1\%$  wt. and in the step 2 (up to  $\approx 834^\circ C$ ) of  $\approx 18.4\%$  wt. The total mass loss produced in the body material was  $\approx 23.5\%$  wt.

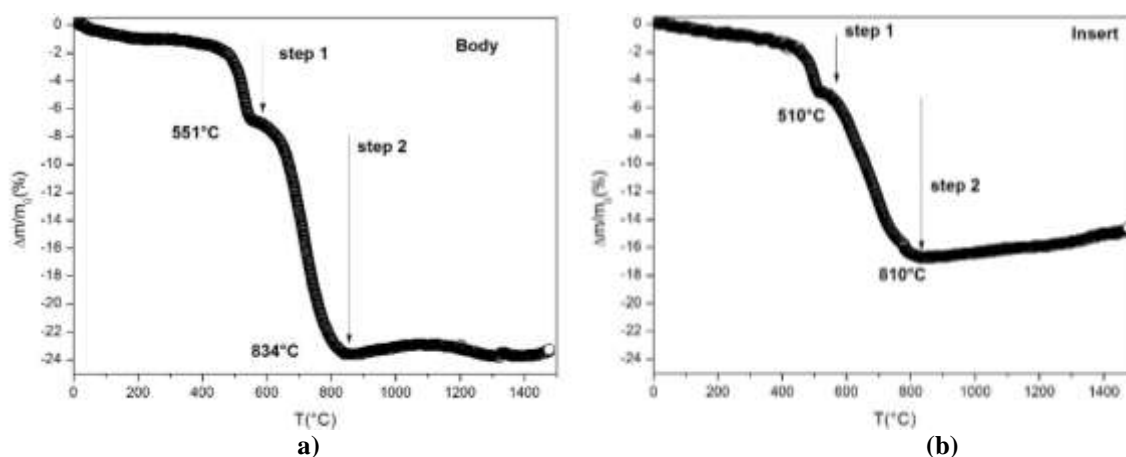


Fig-4: TGA thermograms of the as received nozzle (in air): (a) body material and (b) insert material

The insert material curve showed in Figure 4 (b), also present two steps of mass loss: step 1 (up to  $\approx 510^\circ C$ ) 3.9 % wt. and the step 2 (up to  $\approx 810^\circ C$ ) 12.8 % wt. In this case, the total mass loss result in  $\approx 16.7\%$

wt. The correlation between TGA and DTA curves (Figure 5) shows that the mass loss steps are coincident with two exothermic peaks: around 530°C and 812°C (for the body material) and around 501°C and 810°C

(for the insert material). The two steps allow thinking in the presence of combined reactions. The DTA peaks at  $T < 800^{\circ}\text{C}$  are interpreted as resin transformation (pyrolysis) and the oxidation of “glassy-carbon” reactions. Different types of resins are used in refractories such as Resole, Novolac or epoxy blends. According to Shokralla and Muaikeel [12], the mass loss between  $440 - 580^{\circ}\text{C}$  (step 1) may be due to the breakdown of the methylene linkage group and the last step (step 2) is attributed to thermo-oxidative reactions, that take place at a temperature above  $600^{\circ}\text{C}$ . In the nozzle materials (body and insert) the temperature range of the mentioned reactions are observed between  $T \approx 500^{\circ}\text{C}$  to  $812^{\circ}\text{C}$ . In both cases, the step 2 includes the mass loss due to graphite oxidation. The total mass loss observed in the DTA curves (23.5 %wt. in the body and 16.7 %wt. in the insert) are consistent with the

content of carbon informed in the chemical composition (Table 1).

The body material DTA curve (Figure 5a) shows a peak at  $1170^{\circ}\text{C}$ , which is interpreted as the start of the  $\text{ZrO}_2$  endothermic transformation monoclinic to tetragonal (during heating) and finished at  $1236^{\circ}\text{C}$  in agreement with [13]. The transformation is affected by the  $\text{HfO}_2$  content present in the zircons [2]. This transformation is produced by the content of AZS aggregates present in the body of the nozzle. In the insert curve (Figure 5b), the transformation is not evident because the main crystalline zirconia is cubic stabilized with Ca, in order to avoid the allotropic transformations during service.

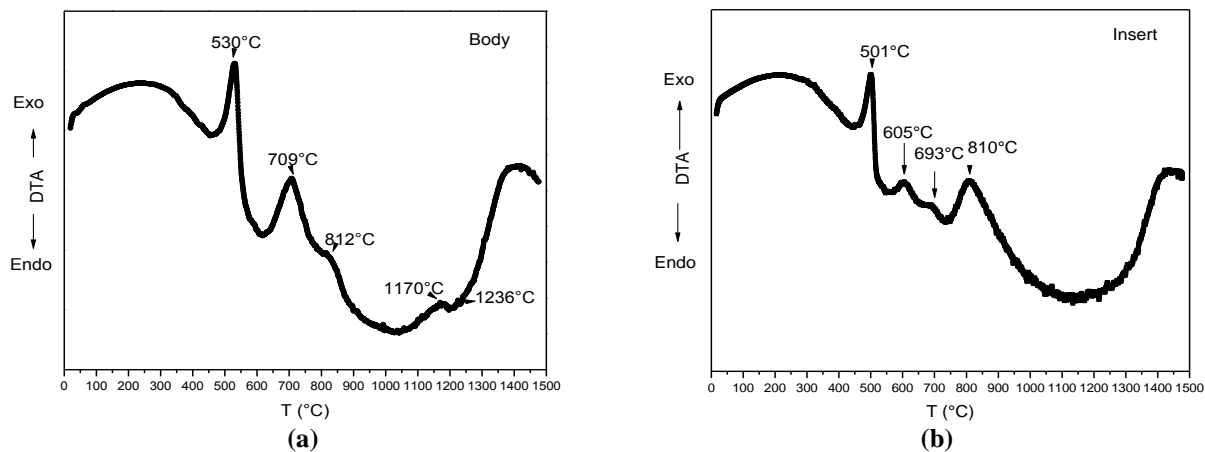


Fig-5: DTA curves of the as received nozzle: (a) body material and (b) insert material

**Mold Fluxes Characterization**

Two mold fluxes with a basicity index (IB) of 0.7 and similar carbon content were selected for the

study: M1 (with 2.6% F) and M2 (without F). The chemical composition is detailed in Table 2.

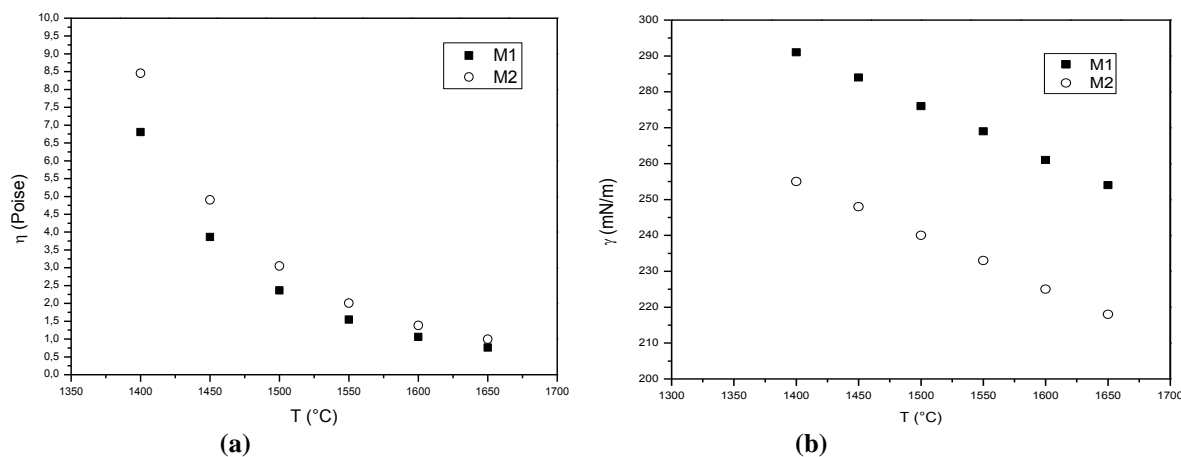
Table 2: Chemical composition of the mold fluxes in (% wt.).

Flux	SiO <sub>2</sub>	CaO	MgO	Al <sub>2</sub> O <sub>3</sub>	Fe <sub>2</sub> O <sub>3</sub>	Na <sub>2</sub> O	K <sub>2</sub> O	F	TiO <sub>2</sub>	Li <sub>2</sub> O	B <sub>2</sub> O <sub>3</sub>	C Total	IB
M1	31.6	22.2	2.1	14.4	3.4	3.7	1.1	2.6	-	-	-	13.7	0.7
M2	39.0	26.9	2.3	17.2	6.5	4.6	0.2	-	0.1	1.3	1.9	13.4	0.7

The physical properties of the mold fluxes, such as viscosity, surface tension and the melting behaviour, were obtained by experimental tests and theoretical calculus. The viscosity was estimated applying a simulation by Fact Sage 7.1. and the surface tension was calculated by the Mills model. Both physical properties were determined considering a temperature range between ( $1400^{\circ}\text{C} - 1650^{\circ}\text{C}$ )

associated with the static corrosion tests and the continuous casting conditions. Figure 6 (a) and (b).




The results shows that both mold fluxes (M1 and M2) present similar viscosity behaviour along the temperature range considered. However, the mold flux M2 shows a slightly lower surface tension than M1. This results allows to predict that M2 could produce higher wettability of the nozzle than M1 flux.



**Fig-6: Physical properties of the mold fluxes M1 and M2: (a) Viscosity (b) Surface tension**

The results of the melting behaviour determined by hot stage microscopy (HSM) for both mold fluxes are observed in Table 3.

**Table 3: Mold fluxes critical temperatures**

Critical Temperature	M1	M2
<b>T softening (°C)</b> 	1195	1125
<b>T hemisphere (°C)</b> 	1206	1130
<b>T fluidity (°C)</b> 	1272	1144

**Corrosion Tests**

Two static corrosion tests were carried out on (as received) nozzle crucibles, in contact with M1 and M2 fluxes. Both tests were performed at 1400°C during 2 h in air. The structural study of the samples was carried out by optical and scanning electron microscopy. The layers of the fluxes adhered on the surface of the crucibles were observed and the thickness of the fluxes layers adhered were determined by SEM analyzed, see Figure (7a) and (7b).

The M2 flux layer thickness is  $\approx 1.23$  mm and in the case of M1 flux the layer thickness is  $\approx 0.71$  mm.

The value of M2 flux layer thickness is justified by the higher viscosity obtained.

The mold flux M2 present a melting behaviour at lower temperatures than M1. On this base it is possible to consider that the liquid phase M2-L infiltrate the insert material more rapidly and take contact with the  $ZrO_2$  aggregates promoting the dissolution of them. The lower surface tension of the flux M2 favored this behaviour. However, the differences in the content of  $ZrO_2$  wt % in the liquid phases between both fluxes (M2-L and M1-L) in relation with temperature is not so relevant. Figure 8.

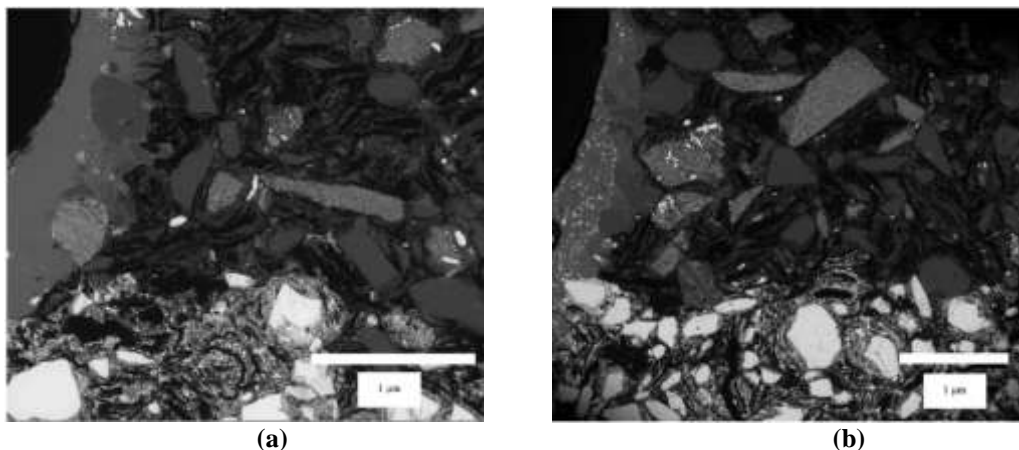


**Fig-7:** Static corrosion tests carried out with mold fluxes M1 and M2; (a) Static corrosion crucible tested with flux M1 and (b) Static corrosion crucible tested with flux M2.

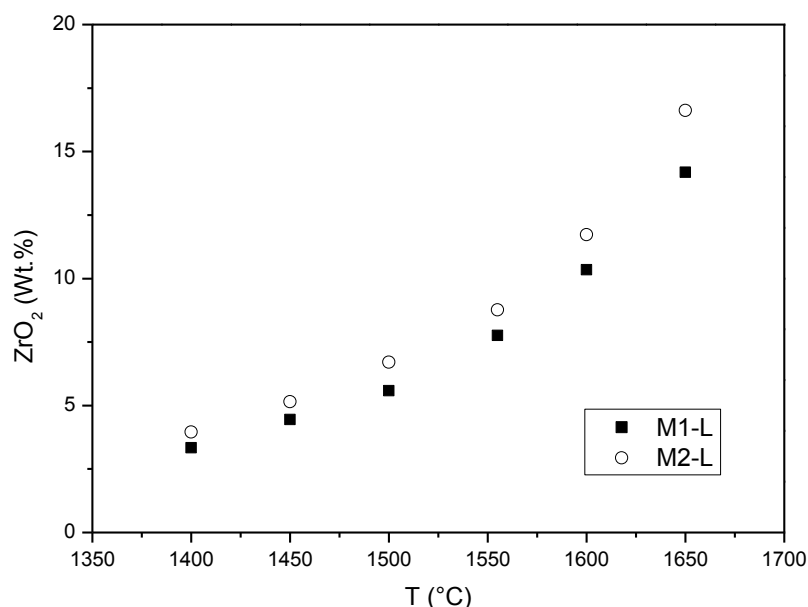


**Fig-8:** ZrO<sub>2</sub> content evolution in the liquid phases of M1 and M2

The EDS analysis, carried out in different zones of the adhered flux layers (M1 and M2), confirm the destabilization of ZrO<sub>2</sub> aggregates of the nozzle insert caused by the calcium content loss of them, in contact with the infiltrated liquid phase. The thermodynamic simulation corroborate that both fluxes between 1400°C and 1650°C generate one liquid phase. The chemical composition in both cases consists in a CaO-MgO-Al<sub>2</sub>O<sub>3</sub>-SiO<sub>2</sub> phase (CMAS system) with Na content. In the case of the M2 the liquid phase in contact with the insert also contains B<sub>2</sub>O<sub>3</sub>.

The liquid phases, in contact with the oxides grain boundaries and sub boundaries promotes

corrosion reactions. CMAS system reacts with the CaO of ZrO<sub>2</sub> grains promoting calcium diffusion to the slag and the allotropic cubic to monoclinic transformation of ZrO<sub>2</sub> structure. Then, monoclinic ZrO<sub>2</sub> particles are eroded by molten slag. As it is possible to observe in Figure 9, the slag is enriched in ZrO<sub>2</sub> content toward the interface with the insert nozzle due to ZrO<sub>2</sub> grains dissolution. A corroded ZrO<sub>2</sub> aggregate is identified because present white spherical particles, see Figure 10. The corrosion mechanisms visualized involves slag infiltration and chemical attack. As is possible to observe the CMAS slag is enriched in Zr content toward the interface with the nozzle material due to ZrO<sub>2</sub> grains dissolution.

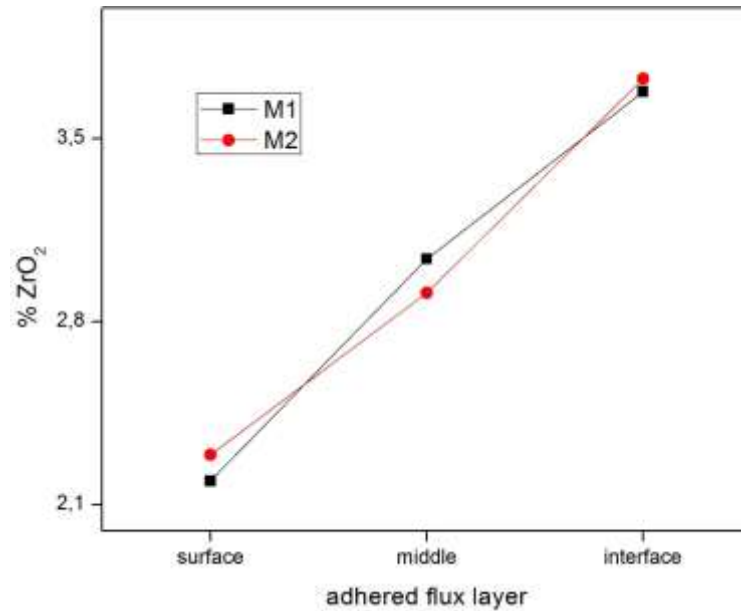


Fig-9: ZrO<sub>2</sub> content in different zones of the adhered flux layer

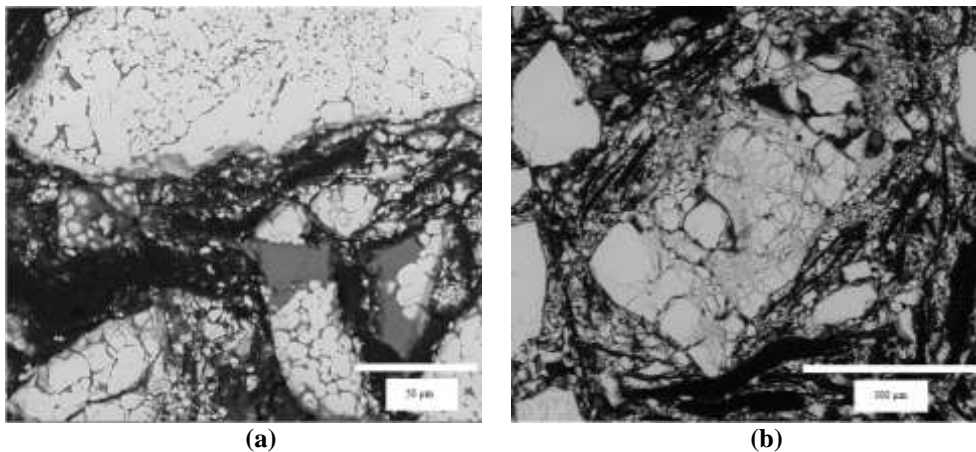


Fig-10: White spherical particle of ZrO<sub>2</sub> corroded in: a) static corrosion crucible with M1 and b) static corrosion crucible with M2

### Post Mortem Study

The post mortem study was carried out to corroborate the impact of M1 at real conditions. The results verified a decrease of  $\approx 8\%$  of the apparent porosity, consistent with the increase of density in the nozzle material after 6 h of casting. On the other hand, the PM sample (Figure 11) presents a smaller adhered flux layer ( $\approx 0.28$  mm) but a bigger mass loss (36.27 %) in comparison with the two static corrosion crucibles. This is justified by the more aggressive and dynamics

industrial conditions that promote more dissolution. Besides, in real conditions the nozzle/flux contact time is longer than in the static corrosion test. For this reason a more intensive chemical attack is promoted. The corrosion mechanisms visualized involves slag infiltration through carbon bond of the nozzle and grains dissolution (Figure 12). In this case, the chemical composition of the adhered slag also consists in CMAS system with Na content.



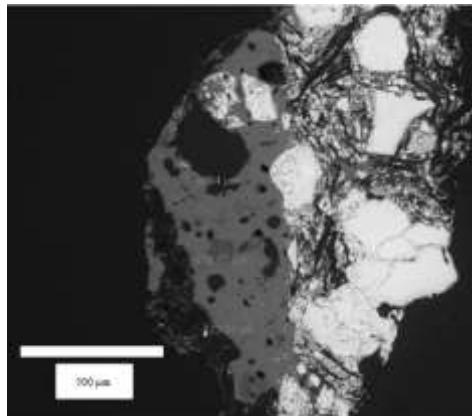


**Fig-11: Adhered slag layer in post mortem nozzle**

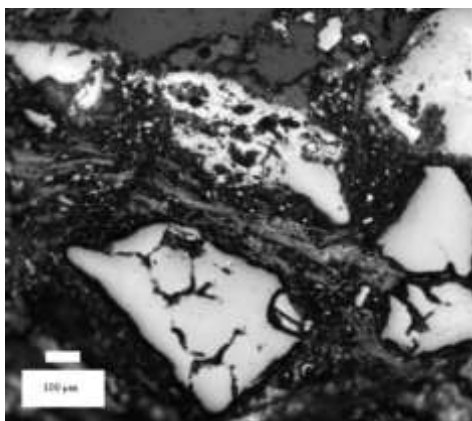


**Fig-12: ZrO<sub>2</sub> grains dissolution**

## CONCLUSIONS

- ✓ The corrosion mechanisms visualized in both cup test and in the post mortem crucible involves: slag infiltration through carbon bond of the nozzle and grains dissolution due to chemical attack.
- ✓ Despite the difference in the chemical composition, the melting behavior and the physical properties (viscosity and surface tension), M1 and M2 mold fluxes presents similar corrosion performance. Then, to avoid the gases emissions and protect the human health as well as the environmental, it is possible take into account M2 as a good free fluorine mold flux substitution to replace the fluorine fluxes used currently in the industry.

## REFERENCES

1. Valentini MA, Brandaleze E. Use of Boron and Lithium oxides as a replacement of fluoride compounds in mold powders, *Scholars Academic Journal of Biosciences (SAJB)*. 2015; 203(3) : 301-308.
2. Sarkar R. *Refractory Technology: Fundamentals and Applications*, CRC Press, Taylor and Francis Group, 2017.
3. Lee WE, Zhang S. Melt Corrosion of oxide and oxide-carbon refractories, *International Materials Reviews*. 1999; 44(3) : 77-104.
4. Mukai K, Toguri JM, Yoshitomi J. Corrosion of alumina-graphite refractories at the slag-metal interface, *Canadian Metallurgical Quarterly*. 1986; 25(4) : 265-275.
5. Hauck F, Potschke J. *Arch. EisenhuttWes.* 1982; 53(4) : 133- xx.
6. Qian F, Li H, Liu G. Formation of Decarbonization Layer and its Effect on Corrosion Resistance of Zirconia Graphite Materials, *Advanced Materials Research*2012; 399-401 : 336-342.
7. Brandaleze E, Benavidez E, Peirani V, Santini L, Gorosurreta C. Impact of free fluor fluxes on nozzle wear mechanisms, *Advances Science and Technology*.2010; 70 : 205-210.
8. Brandaleze E, Peirani V, Avalos M. Mould fluxes viscosity and surface tension influence on the wear mechanisms of Al<sub>2</sub>O<sub>3</sub>-C nozzle, *Advances in Technology*2014; 92 : 226-231.
9. Bale CW, Chartrand P, Decterov SA, Eriksson G, Hack K, Ben Mahfoud R, Melançon J, Pelton AD, Petersen S. *FactSage Thermochemical Software and Databases, CalPhad J*2002; 26 : 189-228.
10. Bale CW, Bélisle E, Chartrand P, Decterov DA, Eriksson G, Hack K, Jung IH, Kang YB, Melançon J, Pelton AD, Robelin C, Petersen S. *Fact Sage Thermochemical Software and Databases-Recent Developments, Calphad*. 2009; 33(2): 135-143.

11. Poirer J, Qafssaoui F, Ildefonse J, Bouchetou M. Analysis and interpretation of refractory microstructures in studies of corrosion mechanisms by liquid oxides, *Journal of European Ceramic Society*. 2008; 28: 1557-1568.
12. Shokralla SA, Muaikel NSA, Ildefonse J, Bouchetou M. Thermal properties of epoxy (DGEBA)/ Phenolic resin (NOVOLAC) Blends, *The Arabian Journal for Science and Engineering*. 2010; 35: 7-14.
13. Gauna MR, Conconi MS, Gomez S, Suárez G, Aglietti EF, Rendtorff NM. Monoclinic-Tetragonal Zirconia Quantification of Commercial nanopowder mixtures by XRD and DTA, *Ceramics – Silikáty*. 2015; 59: 318-325.